

## Article

# Ultrathin-Shelled Zn-AgIn<sub>5</sub>S<sub>8</sub>/ZnS Quantum Dots with Partially Passivated Trap States for Efficient Hydrogen Production

Yanhong Liu <sup>1</sup>, Xianjin Wang <sup>1</sup>, Guan Gong <sup>1</sup>, Afaq Ullah Khan <sup>1</sup>, Geru Li <sup>1</sup>, Tong Ren <sup>1</sup>, Qitao Chen <sup>1</sup>, Lixia Li <sup>2,\*</sup> and Baodong Mao <sup>1,\*</sup>

<sup>1</sup> School of Chemistry and Chemical Engineering, Jiangsu University, Zhenjiang 212013, China

<sup>2</sup> School of Environment and Safety Engineering, Jiangsu University, Zhenjiang 212013, China

\* Correspondence: qingpipa@ujs.edu.cn (L.L.); maobd@ujs.edu.cn (B.M.)

**Abstract:** The manipulation of trap states plays a crucial role in the development of efficient photocatalysts. An ultrathin-shelled Zn-AgIn<sub>5</sub>S<sub>8</sub>/ZnS quantum dots (QDs) photocatalyst was synthesized via in situ growth using a low-temperature hydrothermal method. The optical properties of the samples coated with ZnS shell were studied vis UV-vis absorption and fluorescence spectra. The ultrathin ZnS shell plays an important role in the Zn-AgIn<sub>5</sub>S<sub>8</sub>/ZnS core-shell heterostructure photocatalytic water splitting system, which could reduce surface defects, prolong the carrier lifetime and improve the photo-generated electron-hole pair separation effectively, resulting in the improved photocatalytic efficiency and enhanced stability of the catalyst. The results provide an effective guideline for shell thickness design in future constructions of the core-shell heterostructure photocatalyst.

**Keywords:** I-III-VI QDs; trap states; photocatalysis; hydrogen production



**Citation:** Liu, Y.; Wang, X.; Gong, G.; Khan, A.U.; Li, G.; Ren, T.; Chen, Q.; Li, L.; Mao, B. Ultrathin-Shelled Zn-AgIn<sub>5</sub>S<sub>8</sub>/ZnS Quantum Dots with Partially Passivated Trap States for Efficient Hydrogen Production. *Catalysts* **2024**, *14*, 298. <https://doi.org/10.3390/catal14050298>

Academic Editor: Edward G. Gillan

Received: 27 March 2024

Revised: 22 April 2024

Accepted: 29 April 2024

Published: 30 April 2024



**Copyright:** © 2024 by the authors. Licensee MDPI, Basel, Switzerland. This article is an open access article distributed under the terms and conditions of the Creative Commons Attribution (CC BY) license (<https://creativecommons.org/licenses/by/4.0/>).

## 1. Introduction

Utilizing solar energy for photocatalytic water splitting to produce hydrogen is considered the most ideal way to alleviate energy shortages and prevent ecological damage [1–4]. Due to their excellent biocompatibility, good optical properties and high biochemical stability, multiple I-III-VI nanocrystals or quantum dots (QDs) have been extensively studied in biosensing, light-emitting diodes, solar cells and photocatalytic hydrogen production for nearly a decade [5–13]. The Ag-In-S system, as a typical representative, was further studied in changing the optical properties by regulating the reaction conditions. At present, a large number of studies are devoted to changing the reactant, reaction temperature and reaction time to study changes in optical properties and their corresponding applications [14–17]. Among the applications, photocatalysis attracts a lot of attention due to the advantages of its environmentally friendly, wide range of visible light response and small size to facilitate the diffusion of carriers to the surface [17–19].

In photocatalytic applications, the improvement of the Ag-In-S-based QDs themselves mainly involves the regulation of the proportion of various elements to reduce the bandgap in order to improve visible light absorption [20–22]. Torimoto et al. reported the formation of a structurally controllable (AgIn)<sub>x</sub>Zn<sub>2(1-x)</sub>S<sub>2</sub> solid solution by controlling the ratio of ZnS to AgInS<sub>2</sub>, and they systematically studied the relationship between the bandgap, photocatalytic performance and sample size [23]. At the same time, a large number of studies are devoted to recombining with other semiconductors to construct heterojunctions to promote photogenerated carrier separation and transmission, so these heterojunctions are usually necessary [24–28]. For example, Zhang et al. embedded Zn-Ag-In-S (ZAIS) QDs into 2D NiFe layered double hydroxide nanosheets through simple hydrothermal treatment to form a 0D/2D composite heterojunction system for photo-assisted electrocatalysis. Under light irradiation, for them, the optimized NiFe ZAIS showed a significantly reduced overpotential of 129 mV and 242 mV at current densities of 10 and 50 mA cm<sup>-2</sup>,

22 and 33 mV lower than that of dark electrocatalysis, respectively. Through the proof of transient photovoltage spectroscopy, we have a clear and basic understanding of the dynamics of the charge extraction time and the amount in 0D/2D heterojunction, which has been proven to play a key role in photo-assisted electrocatalysis [29]. On the other hand, although the wide band gap ZnS is an excellent shell material, wrapped I-III-VI QDs to build a core-shell structure can reduce surface defects and improve luminous efficiency, and they are widely used in light-emitting diodes, biological imaging and other fields [30,31]. Sun-synthesized pure blue InP/ZnS quantum dots have an emission wavelength of 468 nm and a quantum yield of 45%. Furthermore, zinc oleate and S-TOP are used as precursors to epitaxially grow the second ZnS shell. The residual zinc stearate reacts with S-TOP to form a ZnS shell, which increases the thickness and stability of QDs. Moreover, as the residual precursor to zinc stearate is removed, the current density increases from 13 mA cm<sup>-2</sup> to 121 mA cm<sup>-2</sup> at 8 V for the hole-only device. External quantum efficiency increased from 0.6% of InP/ZnS quantum dot light-emitting diodes (QLEDs) to 1.7% of InP/ZnS/ZnS QLEDs [32]. However, in the photocatalytic reaction, the type-I band arrangement in this core-shell structure hinders the transfer of photogenerated electrons to the surface of the catalyst [33,34]. In view of this problem, if the structure of the shell material can be reasonably controlled to achieve efficient trap passivation without blocking the charge transfer [35], the unique structure of the interface would make the lifetime of photogenerated carriers significantly increase, they would become thinner, and they would have a short carrier transport distance, resulting in the fast separation of carriers in the interface. Meanwhile, the wide band gap ZnS shell coating also helps improve the stability of the catalyst. However, there is little research on the photocatalytic hydrogen production of ZAIS QDs covering ZnS, and an in-depth understanding of the photocatalyst design and preparation system is lacking.

For the construction of narrow-bandgap photocatalysts, the control of defects or trap states plays a crucial role, which may act as the recombination center of charge carriers, resulting in a decrease in photocatalytic activity [36,37]. However, there are also lots of work that have reported that the trap states can increase the opportunity of charge separation that can result in the enhancement of activity [38,39]. These conflicting results, together with the difficulty of the mechanism's study, make it an ongoing hot topic in the photocatalysis field. As a wide-bandgap and stable semiconductor, ZnS has been employed to construct core-shell nanostructures for surface passivation and defect reduction [40,41]. In order to avoid the decomposition of CdS quantum dots and passivate their surface state, an important strategy of Jin et al. is to grow the "shell" of another semiconductor material to produce core-shell structure quantum dots and physically isolate the active "core" quantum dots from the surrounding environment. Based on density functional theory calculations, ultrafast charge separation rates were ascribed to the formation of an intermediate Au<sub>2</sub>S layer at the semiconductor-metal interface, which can successfully offset the energy confinement introduced via the ZnS shell [42]. This strategy obtained great success in optical applications, such as biological imaging and light-emitting diodes, for which only high-efficiency radiative recombination is required [43,44]. On the contrary, extra consideration is needed for the photovoltaic and photocatalytic processes that require charge separation and collection. It has been reported that shell thickness plays a crucial role in the compromise of defect passivation and the hindering of charge separation via the wide-bandgap ZnS shell [45]. However, activity enhancement is still limited in these core-shell structured photocatalysts, and much work is needed for a better demonstration of the related mechanism.

In this paper, ZAIS/ZnS QDs were synthesized using a simple hydrothermal method at a low temperature, focusing on the effect of a ZnS coating. After the ZnS coating, the light absorption remained basically unchanged, while the photoluminescence (PL) intensity largely increased with a small blue shift of the emission peak. The influence of the ZnS thickness on the photocatalytic activity of the samples and the related mechanism were investigated. It was found that the optimized ZnS shell ratio was only 1.25%. This thin

ZnS shell achieved a decrease in surface defects in the ZAIS/ZnS core-shell structure, but it did not hinder the surface charge separation or improve the photocatalytic efficiency of the key. The average fluorescence lifetime was prolonged, which was mainly due to the decrease in the surface trap state. More importantly, a detailed analysis indicates that ZAIS/ZnS-1.25% actually did not fully passivate the surface defects, which left a certain amount of the fast-decay component, which contributes to an enhanced charge separation and plays a crucial role in high photocatalytic activity. Our work provides new evidence of the core-shell structure design of photocatalysts, suggesting not only that the shell should be thin enough to avoid hindering the charge transfer but also that rapid decay trap states should not be completely eliminated to facilitate charge separation.

## 2. Results and Discussion

To further examine the characteristics of the prepared materials, transmission electron microscope (TEM) and X-ray diffraction (XRD) tests were conducted. Figure 1a shows the XRD spectra of ZAIS QDs and ZAIS/ZnS- $X$  ( $X = 1.25\%$ ,  $5.00\%$  and  $7.50\%$ ) with a core-shell structure. All XRD peaks in Zn-AgIn<sub>5</sub>S<sub>8</sub> QDs were attributed to cubic crystal phase AgIn<sub>5</sub>S<sub>8</sub> (JCPDS No.25-1329) with three main diffraction peaks at  $27.3^\circ$ ,  $46.5^\circ$  and  $55^\circ$ , corresponding to cubic crystal phase AgIn<sub>5</sub>S<sub>8</sub> (311), (440) and (533) facets. Due to the small particle size of the QDs, all the diffraction peaks were relatively wide, and the peak intensity was weak. After the coating of the ZnS shell, the diffraction peak intensity was enhanced, and the crystallinity of the sample was increased, indicating the successful introduction of Zn in the sample [46]. However, no significant movement of the three major diffraction peaks was observed due to the low content of ZnS, and they were similar to the diffraction peak of cubic AgIn<sub>5</sub>S<sub>8</sub>. In Figure 1b, the TEM image illustrates ZAIS/ZnS-1.25% QDs with a uniform distribution and particle sizes ranging from 2 to 5 nm. Moreover, to further elucidate the understanding of ZAIS/ZnS-1.25% QDs, a high-resolution transmission electron microscope (HRTEM) analysis was conducted. Notably, the lattice strip marked with the red circle at 0.32 nm corresponds to the (311) crystal plane of the ZAIS core, while the ZnS shell outside the red circle and within the white circle demonstrates an amorphous lattice structure, as shown in Figure 1c. As depicted in Figure 1d, the HRTEM images exhibit the lattice strip of ZAIS QDs at 0.32 nm.

To investigate the photochemical characteristics of the prepared materials, we conducted UV-vis absorption and PL tests. Figure 2a shows the UV-vis absorption spectra of ZAIS QDs and ZAIS/ZnS- $X$  ( $X = 0.25\%$ ,  $1.25\%$  and  $7.50\%$ ) core-shell heterojunctions. The ZAIS absorption range is in the visible region, and the absorption threshold is about 600 nm. It is soluble in water for the deep red, clear, transparent solution. After the coating of ZnS with a different mass fraction, the absorption range had a small blue shift, and the sample was dissolved in water, showing orange-red. It was shown that the core-shell structure is a ZnS shell formed by coating the surface of Zn, and the light absorption is almost constant [47]. Figure 2b shows the PL spectra of ZAIS QDs and ZAIS/ZnS core-shell heterojunctions. The luminescence intensity of the ZAIS/ZnS core-shell heterojunction was increased after the ZnS coating, and the addition of 0.25%, 1.25% and 7.50% ZnS was 2.17, 2.4 and 1.96 times higher than that of the original QDs. At the same time, the emission peak shifted from 651 nm to 623 nm (ZAIS/ZnS-0.25% and ZAIS/ZnS-1.25%) and 632 nm (ZAIS/ZnS-7.50%). The ZnS coating served to passivate the surface defects of the ZAIS QDs. At lower concentrations of ZnS, this passivation could potentially enhance the luminescence efficiency, causing a blue shift in the emission peak. However, at higher concentrations, the passivation effects may saturate or change, leading to a redshift in the emission peak. Subsequently, we will comprehensively investigate the influence of a ZnS coating on the photocatalytic activity of ZAIS.

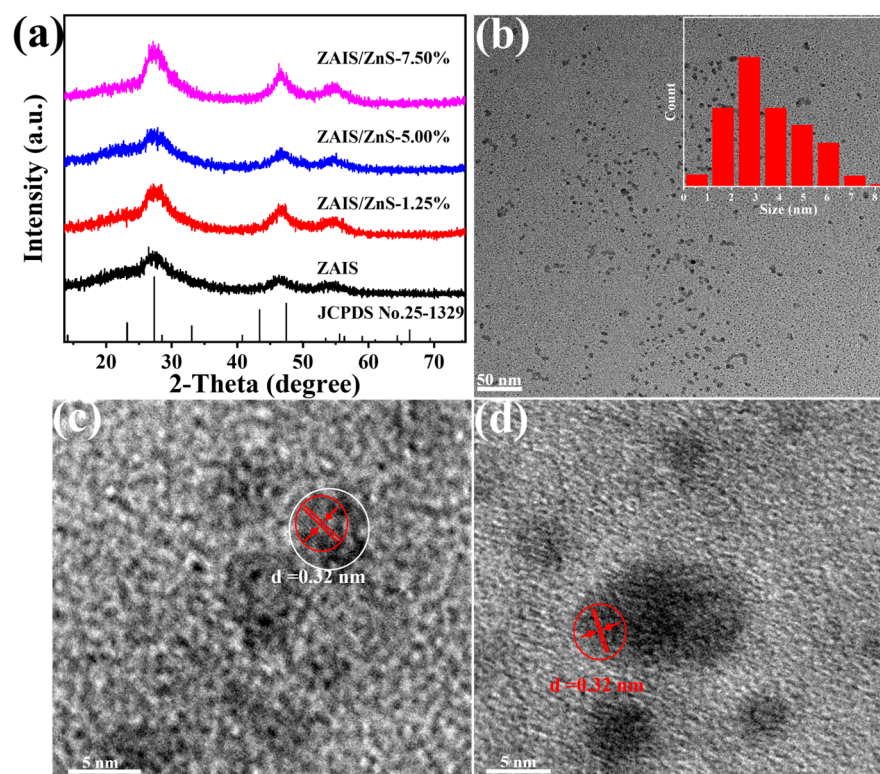


**Figure 1.** (a) XRD patterns of ZAIS QDs and ZAIS/ZnS-X (X = 1.25%, 5.0% and 7.50%) heterojunction with a core-shell structure. TEM (b) and HRTEM (c) images of the ZAIS/ZnS-1.25% sample. Insets (b): size distribution of the ZAIS/ZnS-1.25%. (d) HRTEM images of the ZAIS QDs.

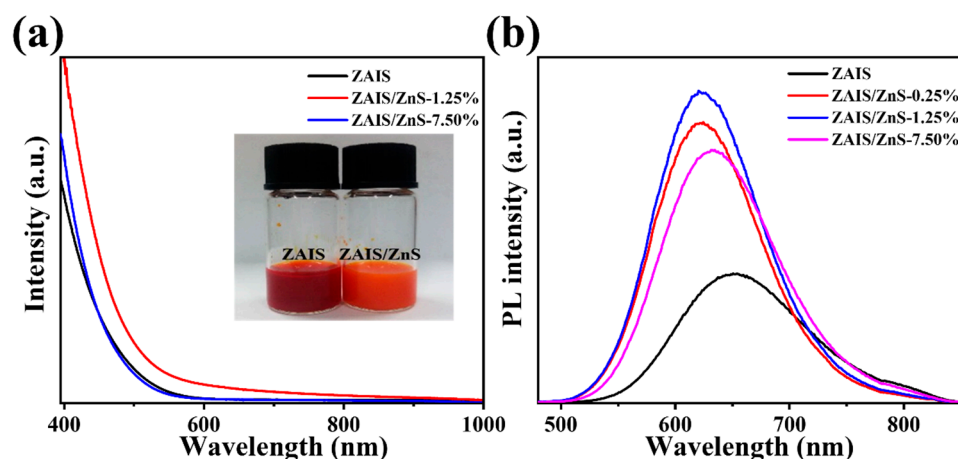


**Figure 2.** (a) UV-vis absorption spectra of the ZAIS QDs and ZAIS/ZnS-X (X = 0.25%, 1.25% and 7.50%) core-shell heterojunction and photographs before and after the ZnS coating. (b) PL spectra of ZAIS QDs and ZAIS/ZnS core-shell heterojunction.

Based on the above discussion of optical properties, to study the activity of ZAIS/ZnS core heterostructure photocatalysts, we determined the ZAIS/ZnS core heterojunctions with different amounts of ZnS ( $1200 \text{ nm} \geq \lambda \geq 420 \text{ nm}$ ) photocatalytic decomposition of water hydrogen production, in which Pt is a co-catalyst. It can be seen from Figure 3a that the hydrogen production at the 5 h of the pure ZAIS QDs in visible light is  $1.240 \text{ mmol g}^{-1}$ , indicating that the ZAIS QDs themselves have good photocatalytic activity, which is attributed to the light response range and a suitable bandgap structure. When the ZnS shell was introduced, the photocatalytic activity of ZAIS/ZnS core-shell heterojunction was significantly improved, and the photocatalytic activity increased with the increase in

the ZnS shell thickness. When the mass ratio of the ZnS shell in the core–shell structure is 1.25%, the hydrogen production reaches 5 h of 4.458 mmol g<sup>-1</sup>. It is suggested that the photocatalytic activity of ZAIS/ZnS core–shell heterojunction is improved, obviously, by covering the ZnS shell, which may be due to the reduction in the core–shell structure, which can effectively reduce the defect state. Figure 3b shows that, with the increase in the ZnS loading from 0 to 1.25%, the corresponding hydrogen production rate of the sample is, from 0.244 mmol g<sup>-1</sup> h<sup>-1</sup>, increased to 0.892 mmol g<sup>-1</sup> h<sup>-1</sup>. When further increasing the amount of coated ZnS to 2.50%, 5.00% and 7.50%, the sample hydrogen production rate decreased slowly but was still higher than the pure ZAIS QDs, which may be because an excessive ZnS coating will hinder the photo-generated electron holes in the catalyst surface transfer, thereby reducing the photocatalytic efficiency. In addition, upon juxtaposing our methodology with those of fellow researchers, discernible advantages of our proposed strategy emerged (Table 1).

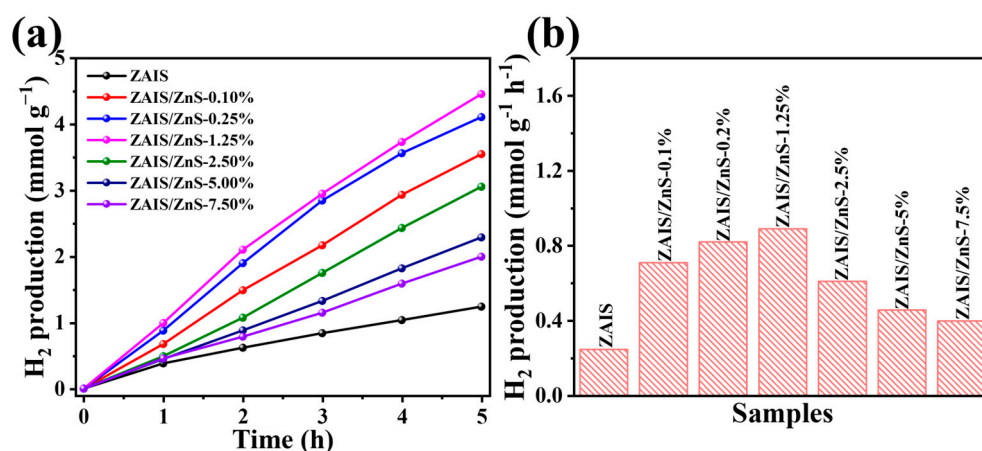


**Figure 3.** (a) Plots of photocatalytic H<sub>2</sub> evolution amount and (b) the production rate of the ZAIS QDs and ZAIS/ZnS core–shell structures with a different capacity of ZnS.

To further study the photocatalytic stability of the samples, cyclic experiments were carried out on the ZAIS/ZnS-1.25% core–shell heterojunctions. The hydrogen production conditions were the same as above. It can be seen from the Figure 4 that the hydrogen production of the ZAIS/ZnS-1.25% photocatalyst was not significantly reduced after 15 h and three rounds of experiments, indicating that the sample has good stability after the ZnS coating.

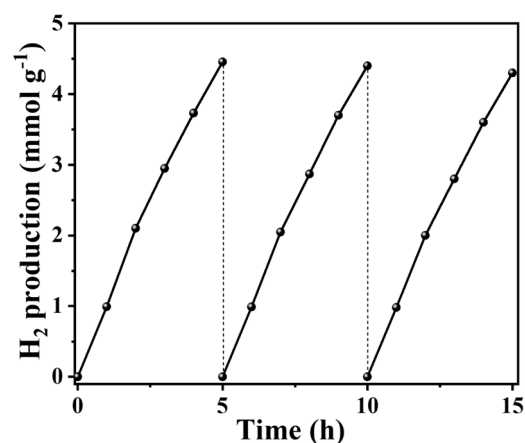


**Figure 4.** Stability study of photocatalytic H<sub>2</sub> production activity over the ZAIS/ZnS-1.25% core–shell heterojunction.

To assess the electrochemical performance and mechanism of the prepared materials, we conducted an EIS test. The electrochemical impedance spectra of ZAIS quantum dots and the ZAIS/ZnS core-shell heterojunction is displayed in Figure 5a. It can be seen from the figure that the impedance arc radius of the ZAIS/ZnS core-shell heterojunction is markedly lower than that of pure ZAIS quantum dots, indicating the enhanced separation efficiency of photogenerated electron-hole pairs due to the ZnS shell coating. Specifically, with a ZnS coating amount of 7.50%, the arc radius is the smallest, indicating that the composite has the highest charge separation efficiency, but the photocatalytic activity is significantly lower than that of ZAIS/ZnS-1.25%. However, it not only indicates that the design process for photocatalytic hydrogen evolution composite can pursue ultra-high charge separation efficiency but also demonstrates the implications of additional factors influencing the photocatalytic hydrogen evolution process.

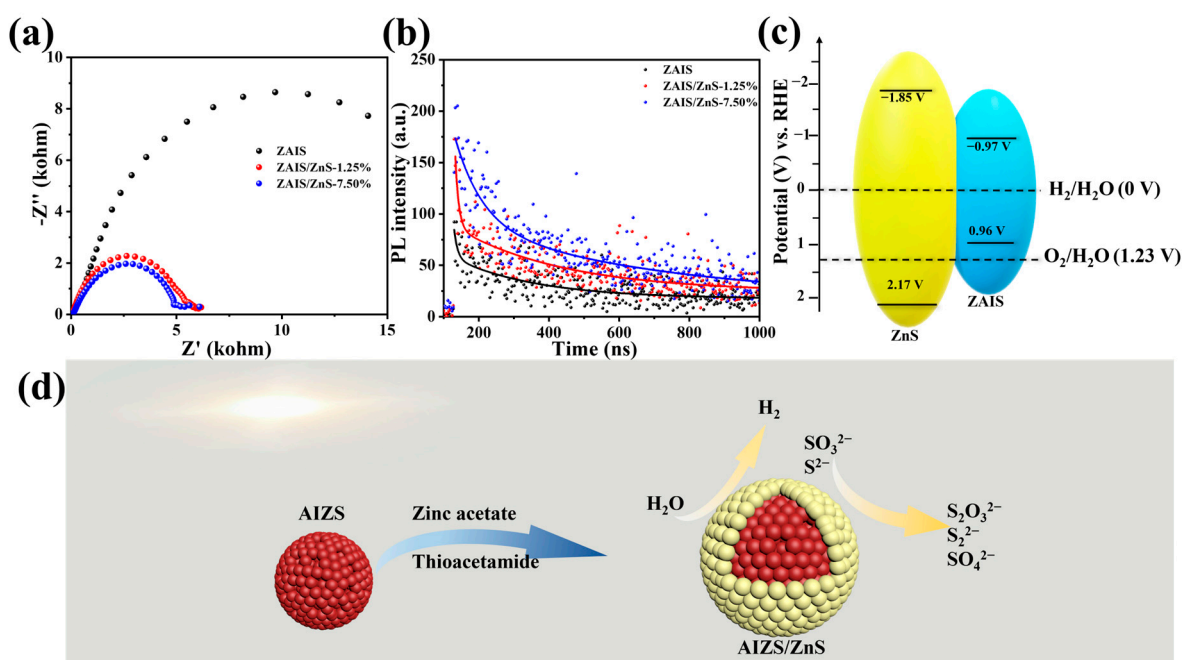


**Figure 5.** (a) Electrochemical impedance of ZAIS and ZAIS/ZnS core-shell QDs. (b) TRPL spectra of ZAIS QDs and ZAIS/ZnS-X (X = 1.25% and 7.50%) core-shell heterojunction. (c) Schematic diagram of energy level levels for ZAIS and ZnS. (d) Photocatalytic hydrogen production mechanism of ZAIS/ZnS core-shell heterojunction.

To further investigate the effect of ZnS coating on the photo-generated electron-hole pair recombination in ZAIS/ZnS, we carried out the characterization of TRPL. Figure 5b shows the fluorescence lifetime spectra of ZAIS QDs and ZAIS/ZnS-X (X = 1.25% and 7.50%) core-shell heterojunctions. The prepared sample was excited at 481 nm and fitted with a double exponential curve,  $I(t) = y_0 + A_1 \cdot \exp(-(t - t_0)/\tau_1) + A_2 \cdot \exp(-(t - t_0)/\tau_2)$ , and the average lifetime was  $\tau_{ave} = (A_1\tau_1 + A_2\tau_2)/(A_1 + A_2)$ . Among them,  $A_1$  and  $A_2$  are the attenuation relative weights, and  $\tau_1$  and  $\tau_2$  are short and long life parameters. In general, the fluorescence lifetime can reflect different electron-hole recombination pathways and mechanisms. After photoexcitation, the photo-generated electrons transition from the conduction band to the surface defect state and the intrinsic defect state. The shorter fluorescence lifetime is attributed to the surface defect state complex; the long fluorescence lifetime is attributed to the eigenstate of the complex [48–50]. The specific parameters for the ZAIS and ZAIS/ZnS core-shell heterojunction fluorescence lifetime is shown in Table 2. It can be seen from the table that the rapid attenuating component  $\tau_1$  were similar at 9.95 ns (ZAIS) and 9.90 ns (ZAIS/ZnS-1.25%) and finally increased to 77.59 (ZAIS/ZnS-7.50%), while the slow attenuation component  $\tau_2$  increased from 238.75 ns (ZAIS) to 316.12 ns (ZAIS/ZnS-1.25%) and 602.42 ns (ZAIS/ZnS-7.50%). The average life expectancy increased

from 156.05 ns to 181.95 ns and 314.41 ns, indicating that photo-generated electrons and holes were effectively separated. The maximum difference of ZnS is that the surface life of ZAIS/ZnS-1.25% is similar to that of ZAIS, which indicates that the ultrathin ZnS shell has not been completely wrapped on its surface. Meanwhile, the surface life of ZAIS/ZnS-7.50% is significantly prolonged, indicating a significant change in surface properties. Compared with the photocatalytic performance diagram of Figure 3, the coated ZnS can effectively suppress the electron–hole nonradiative recombination, but the shell is too thick to bind electrons when the photo-generated electrons are not easily migrated, so the ZAIS/ZnS core of the optimized ZnS coating is 1.25%, and it can reduce the defects and enable photogenerated electrons and holes to effectively transfer.

**Table 1.** Comparison of hydrogen production of the related photocatalysts.

Catalysts	Light Source	Reaction Conditions	H <sub>2</sub> Evolution Rate ( $\mu\text{mol g}^{-1} \text{h}^{-1}$ )	Ref.
ZAIS/ZnS	$\lambda \geq 420 \text{ nm}$	0.35 M Na <sub>2</sub> S + 0.25 M Na <sub>2</sub> SO <sub>3</sub>	892.0	This work
ZAIS/RGO	$\lambda \geq 400 \text{ nm}$	0.35 M Na <sub>2</sub> S + 0.25 M Na <sub>2</sub> SO <sub>3</sub>	342.3	[51]
Cu/ZnS/COF	$\lambda \geq 220 \text{ nm}$	Formic acid	278.4	[52]
CdS/ZnS core–shell	$\lambda \geq 430 \text{ nm}$	0.35 M Na <sub>2</sub> S + 0.25 M Na <sub>2</sub> SO <sub>3</sub>	55.5	[53]
Cu-Doped ZnS	$\lambda \geq 420 \text{ nm}$	0.35 M Na <sub>2</sub> S + 0.25 M Na <sub>2</sub> SO <sub>3</sub>	283.8	[54]
g-C <sub>3</sub> N <sub>4</sub> /ZnS	$\lambda \geq 400 \text{ nm}$	Glucose solution	69.8	[55]
ZnS(en) <sub>0.5</sub> -CdS	$\lambda \geq 400 \text{ nm}$	0.18 M Na <sub>2</sub> S	559.0	[56]

**Table 2.** Exponential decay-fitting parameters of TRPL for samples.

	ZAIS	ZAIS/ZnS-1.25%	ZAIS/ZnS-7.50%
A <sub>1</sub> /%	36.10	43.81	54.87
$\tau_1$ /ns	9.95	9.90	77.59
A <sub>2</sub> /%	63.90	56.19	45.13
$\tau_2$ /ns	238.75	316.12	602.42
$\tau_{ave}$ /ns	156.05	181.95	314.41

According to the previous work of our group and other related literature [51,57], we drew energy level diagrams for ZAIS and ZnS (Figure 5c). It can be seen that its energy level structure is a typical type I heterojunction, which is conducive to promoting charge separation and enhancing photocatalytic activity. Based on the above research, the photocatalytic mechanism of ZAIS/ZnS is shown in Figure 5d. By utilizing the ZAIS core wrapped in an ultra-thin ZnS shell, defects in ZAIS that serve as photo-generated carrier recombination centers are twisted into fast-decay trap states in ZAIS/ZnS composite materials, thereby promoting charge separation and improving photocatalytic hydrogen evolution efficiency [58,59]. Specifically, on the one hand, photo-generated electrons react rapidly with H<sub>2</sub>O to generate hydrogen; on the other hand, photo-generated holes are quickly captured via the sacrificial agents Na<sub>2</sub>SO<sub>3</sub> and Na<sub>2</sub>S.

### 3. Experimental Procedure

#### 3.1. Chemical Reagents

Silver nitrate (AgNO<sub>3</sub>), zinc acetate (Zn(OAc)<sub>2</sub>·2H<sub>2</sub>O), indium nitrate (In(NO<sub>3</sub>)<sub>3</sub>·4.5H<sub>2</sub>O), thioacetamide (TAA), L-cysteine, sodium hydroxide (NaOH), thiourea (CH<sub>4</sub>N<sub>2</sub>S), sodium sulfite (Na<sub>2</sub>SO<sub>3</sub>), sodium sulfide (Na<sub>2</sub>S) and absolute ethanol were purchased from Sinopharm Chemical Reagent Co., Ltd., Shanghai, China. All chemicals were analytical-grade and used without further purification.

#### 3.2. Synthesis of Zn-AgIn<sub>5</sub>S<sub>8</sub> QDs

Pristine Zn-AgIn<sub>5</sub>S<sub>8</sub> QDs were prepared using a simple hydrothermal method according to the previous work [27], and the ratio of Ag:In:Zn in the precursor was controlled at

2:10:5. In a typical synthesis process, 0.34 mmol of  $\text{AgNO}_3$ , 1.7 mmol of  $\text{In}(\text{NO}_3)_3 \cdot 4.5\text{H}_2\text{O}$  and 0.85 mmol of  $\text{Zn}(\text{OAc})_2 \cdot 2\text{H}_2\text{O}$  were added into 5.5 mL of deionized water and stirred until dissolved completely to obtain a clear solution. After that, 2 mL of 2.5 M L-cysteine was added via ultrasonic mixing, and then the pH of the mixed solution was adjusted to 8.5 with a 1 M NaOH solution. Finally, 6.5 mL of a 0.5 M TAA solution was added through vigorous stirring, and the mixture was transferred to a 50 mL Teflon-lined stainless-steel autoclave and kept in a 110 °C oven for 4 h. The QDs product was precipitated out with ethanol and washed three times with water and ethanol to obtain the Zn-AgIn<sub>5</sub>S<sub>8</sub> QDs. The obtained QDs were dispersed in water for further storage and characterization.

### 3.3. Synthesis of Zn-AgIn<sub>5</sub>S<sub>8</sub>/ZnS QDs

Zn-AgIn<sub>5</sub>S<sub>8</sub>/ZnS QDs was synthesized via the in situ growth of a core-shell structure. Specifically, 0.2 g of the Zn-AgIn<sub>5</sub>S<sub>8</sub> sample was dispersed in 20 mL of deionized water and mixed with a certain amount of 0.1 M  $\text{Zn}(\text{OAc})_2 \cdot 2\text{H}_2\text{O}$  solution and a corresponding amount of 0.1 M TAA for 20 min. The mixed solution was transferred to a 50 mL Teflon-lined stainless-steel autoclave and kept at 110 °C in an oven for 4 h. After cooling down to room temperature, the hydrothermal reaction product was washed three times with water and anhydrous ethanol to create ZAIS/ZnS QDs like those of the pristine ZAIS QDs. The loading amount of ZnS was controlled at 0.10%, 0.25%, 1.25%, 2.50%, 5.00% and 7.50%, respectively.

### 3.4. Characterizations

The powder XRD patterns were recorded using an X-ray diffractometer (D8 ADVANCE, Bruker, Berlin, Germany) with  $\text{Cu-K}\alpha$  ( $\lambda = 1.54056 \text{ \AA}$ ) radiation at a scanning rate of 5 °/min. The morphology and size were tested using Tecnai G2 F30 S-Twin (FEI) TEM with an accelerating voltage of 300 kV. The PL spectra of these samples were analyzed on a Cary Eclipse fluorescence spectrophotometer with an excitation wavelength of 450 nm. UV-vis absorption spectra were recorded on a Cary 8454 spectrophotometer. Time-resolved PL (TRPL) spectra were recorded using a QuantaMaster™ 40 spectrometer (Photon Technology International, Inc., Birmingham, NJ, USA) excited at 481 nm. The electrochemical impedance (EIS) spectra were carried out on a CHI 760E electrochemical workstation (CH Instruments, Inc., Shanghai, China) with a standard three-electrode cell at room temperature.

### 3.5. Photocatalytic Hydrogen Production Experiment

Photocatalytic H<sub>2</sub> production was carried out in a Lab-H<sub>2</sub> photocatalytic system with a 300 W xenon lamp and a cutoff filter ( $1200 \text{ nm} \geq \lambda \geq 420 \text{ nm}$ ) as the light source. In a typical experiment, 50 mg of the photocatalysts was dispersed in 100 mL of 0.25 M  $\text{Na}_2\text{SO}_3$  and a 0.35 M  $\text{Na}_2\text{S}$  aqueous solution as the sacrificial reagents and stirred continuously to ensure the uniform irradiation of the catalyst suspension during the whole experiment. Prior to the photocatalytic reaction, the  $\text{H}_2\text{PtCl}_6 \cdot 6\text{H}_2\text{O}$  solution was dripped into the system to photodeposit 2 wt% of Pt nanoparticles onto the photocatalyst surface as the co-catalyst. Before irradiation, the system was vacuumed for 20 min to remove dissolved oxygen in the solution. During the photocatalytic reaction process, a certain amount of the evolved gas was collected per hour and analyzed with an online gas chromatograph (Tianmei, GC-7900, TCD detector, Shanghai, China) using argon as the carrier gas.

## 4. Conclusions

A series of ZAIS/ZnS core-shell heterojunction photocatalysts was synthesized via in situ growth with a low-temperature hydrothermal treatment. Different amounts of  $\text{Zn}(\text{OAc})_2$  were introduced to pre-synthesized ZAIS QDs for the preparation of ZAIS/ZnS core-shell structures with a controllable ZnS shell using a hydrothermal method at a low temperature of 110 °C. The optical properties, transient fluorescence and electrochemical impedance of the samples coated with the ZnS shell were studied via XRD, and the mechanism of photogenerated electron-hole recombination was studied based on the

crystallinity and purity, UV-vis absorption and fluorescence spectra of the samples. It was found that the ZnS shell plays an important role in the photocatalytic hydrogen production activity of the ZAIS/ZnS core-shell structures. The ZnS shell can reduce surface defects and prolong the carrier lifetime, as well as the electron-hole pair separation efficiency, thereby enhancing the photocatalytic activity and improving the catalyst stability. However, the effect of excess ZnS shell thickness on hydrogen production efficiency was found to be 1.25% of the best mass ratio. More importantly, it was found that this low ZnS coating resulted in a partial remainder of the fast-decay trap states, which provides an important contribution to charge separation instead of acting as the recombination center. As trap states manipulation plays a crucial role in narrow-bandgap photocatalysts, our work here provides an important guideline for the future construction of core-shell heterojunction photocatalysts with a high visible light response, efficient charge separation and low charge recombination.

**Author Contributions:** Y.L.: conceptualization, data curation, formal analysis, investigation, methodology and writing—original draft. X.W.: formal analysis, investigation and writing—original draft. G.G.: formal analysis and investigation. A.U.K.: validation, funding acquisition and writing—review and editing. G.L. and T.R.: conceptualization, investigation and methodology. Q.C.: investigation, writing—original draft and formal analysis. L.L.: investigation and supervision. B.M.: conceptualization, project administration, funding acquisition, supervision and writing—review and editing. All authors have read and agreed to the published version of the manuscript.

**Funding:** This work was supported by the National Natural Science Foundation of China (22278194, 21908081) and the Jiangsu Provincial Excellent Postdoctoral Program (2023ZB856).

**Data Availability Statement:** No data were used for the research described in this article.

**Conflicts of Interest:** The authors declare no competing financial interests.

## References

1. Zhou, P.; Navid, I.A.; Ma, Y.; Xiao, Y.; Wang, P.; Ye, Z.; Zhou, B.; Sun, K.; Mi, Z. Solar-to-hydrogen efficiency of more than 9% in photocatalytic water splitting. *Nature* **2023**, *613*, 66–70. [[CrossRef](#)] [[PubMed](#)]
2. Zhang, L.; Zhang, J.; Yu, H.; Yu, J. Emerging S-Scheme Photocatalyst. *Adv. Mater.* **2022**, *34*, 2107668. [[CrossRef](#)] [[PubMed](#)]
3. Tao, X.; Zhao, Y.; Wang, S.; Li, C.; Li, R. Recent advances and perspectives for solar-driven water splitting using particulate photocatalysts. *Chem. Soc. Rev.* **2022**, *51*, 3561–3608. [[CrossRef](#)] [[PubMed](#)]
4. Wang, Y.; Zhang, Y.; Xin, X.; Yang, J.; Wang, M.; Wang, R.; Guo, P.; Huang, W.; Sobrido, A.J.; Wei, B.; et al. In situ photocatalytically enhanced thermogalvanic cells for electricity and hydrogen production. *Science* **2023**, *381*, 291–296. [[CrossRef](#)] [[PubMed](#)]
5. Chong, W.-K.; Ng, B.-J.; Lee, Y.J.; Tan, L.-L.; Putri, L.K.; Low, J.; Mohamed, A.R.; Chai, S.-P. Self-activated superhydrophilic green ZnIn<sub>2</sub>S<sub>4</sub> realizing solar-driven overall water splitting: Close-to-unity stability for a full daytime. *Nat. Commun.* **2023**, *14*, 7676–7688. [[CrossRef](#)] [[PubMed](#)]
6. Liu, B.; Li, X.; Zhao, Q.; Ke, J.; Tadé, M.; Liu, S. Preparation of AgInS<sub>2</sub>/TiO<sub>2</sub> composites for enhanced photocatalytic degradation of gaseous o-dichlorobenzene under visible light. *Appl. Catal. B* **2016**, *185*, 1–10. [[CrossRef](#)]
7. Ruan, X.; Meng, D.; Huang, C.; Xu, M.; Jiao, D.; Cheng, H.; Cui, Y.; Li, Z.; Ba, K.; Xie, T.; et al. Artificial Photosynthetic System with Spatial Dual Reduction Site Enabling Enhanced Solar Hydrogen Production. *Adv. Mater.* **2023**, *36*, 2309199–2309208. [[CrossRef](#)] [[PubMed](#)]
8. Lu, P.; Liu, K.; Liu, Y.; Ji, Z.; Wang, X.; Hui, B.; Zhu, Y.; Yang, D.; Jiang, L. Heterostructure with tightly-bound interface between In<sub>2</sub>O<sub>3</sub> hollow fiber and ZnIn<sub>2</sub>S<sub>4</sub> nanosheet toward efficient visible light driven hydrogen evolution. *Appl. Catal. B* **2024**, *345*, 123697–123705. [[CrossRef](#)]
9. Stroyuk, O.; Raevskaya, A.; Gaponik, N. Solar light harvesting with multinary metal chalcogenide nanocrystals. *Chem. Soc. Rev.* **2018**, *47*, 5354–5422. [[CrossRef](#)]
10. Sun, P.; Xing, Z.; Li, Z.; Zhou, W. Recent advances in quantum dots photocatalysts. *Chem. Eng. J.* **2023**, *458*, 141399–141423. [[CrossRef](#)]
11. Yadav, S.; Yashas, S.R.; Shivaraju, H.P. Transitional metal chalcogenide nanostructures for remediation and energy: A review. *Environ. Chem. Lett.* **2021**, *19*, 3683–3700. [[CrossRef](#)]
12. Li, S.; Tang, X.; Zang, Z.; Yao, Y.; Yao, Z.; Zhong, H.; Chen, B. I-III-VI chalcogenide semiconductor nanocrystals: Synthesis, properties, and applications. *Chin. J. Catal.* **2018**, *39*, 590–605. [[CrossRef](#)]
13. Mamiyev, Z.; Balayeva, N.O. Metal Sulfide Photocatalysts for Hydrogen Generation: A Review of Recent Advances. *Catalysts* **2022**, *12*, 1316. [[CrossRef](#)]

14. Lin, H.; Yang, J.; Liu, Y.-F.; Zeng, F.-J.; Tang, X.-S.; Yao, Z.-Q.; Guan, H.-L.; Xiong, Q.; Zhou, J.-E.; Wu, D.-F.; et al. Stable and efficient hybrid Ag-In-S/ZnS@SiO<sub>2</sub>-carbon quantum dots nanocomposites for white light-emitting diodes. *Chem. Eng. J.* **2020**, *393*, 124654–124662. [[CrossRef](#)]
15. Azhniuk, Y.M.; Gomonnai, A.V.; Solonenko, D.; Lopushansky, V.V.; Loya, V.Y.; Voynarovych, I.M.; Roman, I.Y.; Zahn, D.R.T. Characterization of Ag-In-S films prepared by thermal evaporation. *Mater. Today Proc.* **2022**, *62*, 5745–5748. [[CrossRef](#)]
16. Zhang, J.; Fan, T.; Huang, P.; Lian, X.; Guo, Y.; Chen, Z.; Yi, X. Electro-Reconstruction-Induced Strain Regulation and Synergism of Ag-In-S toward Highly Efficient CO<sub>2</sub> Electrolysis to Formate. *Adv. Funct. Mater.* **2022**, *32*, 2113075–2113086. [[CrossRef](#)]
17. Li, F.; Liu, Y.; Chen, Q.; Gu, X.; Dong, W.; Zhang, D.; Huang, H.; Mao, B.; Kang, Z.; Shi, W. Transient photovoltage study of the kinetics and synergy of electron/hole co-extraction in MoS<sub>2</sub>/Ag-In-Zn-S/carbon dot photocatalysts for promoted hydrogen production. *Chem. Eng. J.* **2022**, *439*, 135759–135770. [[CrossRef](#)]
18. Yuan, Y.-J.; Chen, D.-Q.; Xiong, M.; Zhong, J.-S.; Wan, Z.-Y.; Zhou, Y.; Liu, S.; Yu, Z.-T.; Yang, L.-X.; Zou, Z.-G. Bandgap engineering of (AgIn)<sub>x</sub>Zn<sub>2(1-x)</sub>S<sub>2</sub> quantum dot photosensitizers for photocatalytic H<sub>2</sub> generation. *Appl. Catal. B* **2017**, *204*, 58–66. [[CrossRef](#)]
19. Yang, J.; Fu, H.; Yang, D.; Gao, W.; Cong, R.; Yang, T. ZnGa<sub>2-x</sub>In<sub>x</sub>S<sub>4</sub> (0 ≤ x ≤ 0.4) and Zn<sub>1-2y</sub>(CuGa)<sub>y</sub>Ga<sub>1.7</sub>In<sub>0.3</sub>S<sub>4</sub> (0.1 ≤ y ≤ 0.2): Optimize Visible Light Photocatalytic H<sub>2</sub> Evolution by Fine Modulation of Band Structures. *Inorg. Chem.* **2015**, *54*, 2467–2473. [[CrossRef](#)]
20. Shi, L.; Ren, X.; Zhang, Z.; Wang, Q.; Li, Y.; Ye, J. Non-stoichiometric Ag-In-S quantum dots for efficient photocatalytic CO<sub>2</sub> reduction: Ag/In molar ratio dependent activity and selectivity. *J. Catal.* **2021**, *401*, 271–278. [[CrossRef](#)]
21. Zeng, B.; Chen, F.; Liu, Z.; Guan, Z.; Li, X.; Teng, F.; Tang, A. Seeded-mediated growth of ternary Ag-In-S and quaternary Ag-In-Zn-S nanocrystals from binary Ag<sub>2</sub>S seeds and the composition-tunable optical properties. *J. Mater. Chem. C* **2019**, *7*, 1307–1315. [[CrossRef](#)]
22. Kameyama, T.; Kishi, M.; Miyamae, C.; Sharma, D.K.; Hirata, S.; Yamamoto, T.; Uematsu, T.; Vacha, M.; Kuwabata, S.; Torimoto, T. Wavelength-Tunable Band-Edge Photoluminescence of Nonstoichiometric Ag-In-S Nanoparticles via Ga<sup>3+</sup> Doping. *ACS Appl. Mater. Interfaces* **2018**, *10*, 42844–42855. [[CrossRef](#)] [[PubMed](#)]
23. Kameyama, T.; Takahashi, T.; Machida, T.; Kamiya, Y.; Yamamoto, T.; Kuwabata, S.; Torimoto, T. Controlling the Electronic Energy Structure of ZnS-AgInS<sub>2</sub> Solid Solution Nanocrystals for Photoluminescence and Photocatalytic Hydrogen Evolution. *J. Phys. Chem. C* **2015**, *119*, 24740–24749. [[CrossRef](#)]
24. Li, F.; Xia, Z.; Liu, Q. Controllable Synthesis and Optical Properties of ZnS:Mn<sup>2+</sup>/ZnS/ZnS:Cu<sup>2+</sup>/ZnS Core/Multishell Quantum Dots toward Efficient White Light Emission. *ACS Appl. Mater. Interfaces* **2017**, *9*, 9833–9839. [[CrossRef](#)] [[PubMed](#)]
25. Reddy, N.L.; Rao, V.N.; Kumari, M.M.; Sathish, M.; Muthukonda Venkatakrishnan, S. Development of high quantum efficiency CdS/ZnS core/shell structured photocatalyst for the enhanced solar hydrogen evolution. *Int. J. Hydrogen Energy* **2018**, *43*, 22315–22328. [[CrossRef](#)]
26. Chen, Q.; Liu, Y.; Mao, B.; Wu, Z.; Yan, W.; Zhang, D.; Li, Q.; Huang, H.; Kang, Z.; Shi, W. Carbon-Dot-Mediated Highly Efficient Visible-Driven Photocatalytic Hydrogen Evolution Coupled with Organic Oxidation. *Adv. Funct. Mater.* **2023**, *33*, 2305318. [[CrossRef](#)]
27. Li, F.; Liu, Y.; Mao, B.; Li, L.; Huang, H.; Zhang, D.; Dong, W.; Kang, Z.; Shi, W. Carbon-dots-mediated highly efficient hole transfer in I-III-VI quantum dots for photocatalytic hydrogen production. *Appl. Catal. B* **2021**, *292*, 120154. [[CrossRef](#)]
28. Chen, Q.; Liu, Y.; Gu, X.; Li, D.; Zhang, D.; Zhang, D.; Huang, H.; Mao, B.; Kang, Z.; Shi, W. Carbon dots mediated charge sinking effect for boosting hydrogen evolution in Cu-In-Zn-S QDs/MoS<sub>2</sub> photocatalysts. *Appl. Catal. B* **2022**, *301*, 120755–120767. [[CrossRef](#)]
29. Zhang, D.; Dong, W.; Liu, Y.; Gu, X.; Yang, T.; Hong, Q.; Li, D.; Zhang, D.; Zhou, H.; Huang, H.; et al. Ag-In-Zn-S Quantum Dot-Dominated Interface Kinetics in Ag-In-Zn-S/NiFe LDH Composites toward Efficient Photoassisted Electrocatalytic Water Splitting. *ACS Appl. Mater. Interfaces* **2021**, *13*, 42125–42137. [[CrossRef](#)]
30. Cui, C.; Fu, J.; Kou, D.; Li, Y.; Wei, H.; Wu, Z.; Zhou, W.; Zhou, Z.; Yuan, S.; Qi, Y.; et al. Heterojunction reconstruction via In doping towards high-efficiency CZTSSe solar cells. *Chem. Eng. J.* **2023**, *476*, 146701–146708. [[CrossRef](#)]
31. Benayas, A.; Ren, F.; Carrasco, E.; Marzal, V.; del Rosal, B.; Gonfa, B.A.; Juarranz, Á.; Sanz-Rodríguez, F.; Jaque, D.; García-Solé, J.; et al. PbS/CdS/ZnS Quantum Dots: A Multifunctional Platform for In Vivo Near-Infrared Low-Dose Fluorescence Imaging. *Adv. Funct. Mater.* **2015**, *25*, 6650–6659. [[CrossRef](#)]
32. Zhang, W.; Ding, S.; Zhuang, W.; Wu, D.; Liu, P.; Qu, X.; Liu, H.; Yang, H.; Wu, Z.; Wang, K.; et al. InP/ZnS/ZnS Core/Shell Blue Quantum Dots for Efficient Light-Emitting Diodes. *Adv. Funct. Mater.* **2020**, *30*, 2005303. [[CrossRef](#)]
33. Li, X.; Chen, Y.; Tao, Y.; Shen, L.; Xu, Z.; Bian, Z.; Li, H. Challenges of photocatalysis and their coping strategies. *Chem Catal.* **2022**, *2*, 1315–1345. [[CrossRef](#)]
34. Xu, Q.; Zhang, L.; Cheng, B.; Fan, J.; Yu, J. S-Scheme Heterojunction Photocatalyst. *Chem* **2020**, *6*, 1543–1559. [[CrossRef](#)]
35. Wu, K.; Lian, T. Quantum confined colloidal nanorod heterostructures for solar-to-fuel conversion. *Chem. Soc. Rev.* **2016**, *45*, 3781–3810. [[CrossRef](#)]
36. Ahmad, I.; Zou, Y.; Yan, J.; Liu, Y.; Shukrullah, S.; Naz, M.Y.; Hussain, H.; Khan, W.Q.; Khalid, N.R. Semiconductor photocatalysts: A critical review highlighting the various strategies to boost the photocatalytic performances for diverse applications. *Adv. Colloid Interface Sci.* **2023**, *311*, 102830–102852. [[CrossRef](#)]
37. Liu, K.; Zhang, B.; Zhang, J.; Lin, W.; Wang, J.; Xu, Y.; Xiang, Y.; Hisatomi, T.; Domen, K.; Ma, G. Synthesis of Narrow-Band-Gap GaN:ZnO Solid Solution for Photocatalytic Overall Water Splitting. *ACS Catal.* **2022**, *12*, 14637–14646. [[CrossRef](#)]

38. Hinterding, S.O.M.; Salzmann, B.B.V.; Vonk, S.J.W.; Vanmaekelbergh, D.; Weckhuysen, B.M.; Hutter, E.M.; Rabouw, F.T. Single Trap States in Single CdSe Nanoplatelets. *ACS Nano* **2021**, *15*, 7216–7225. [[CrossRef](#)]
39. Wang, T.; Xu, L.; Cui, J.; Wu, J.; Li, Z.; Wu, Y.; Tian, B.; Tian, Y. Enhanced Charge Separation for Efficient Photocatalytic H<sub>2</sub> Production by Long-Lived Trap-State-Induced Interfacial Charge Transfer. *Nano Lett.* **2022**, *22*, 6664–6670. [[CrossRef](#)]
40. Long, Z.; Yang, G.; Shao, R.; Chen, Z.; Liu, Y.; Liu, R.; Zhong, H. The Strain Effects and Interfacial Defects of Large ZnSe/ZnS Core/Shell Nanocrystals. *Small* **2023**, *20*, 2306602–2306610. [[CrossRef](#)]
41. Huang, R.-J.; Qin, Z.-K.; Shen, L.-L.; Lv, G.; Tao, F.; Wang, J.; Gao, Y.-J. Interface engineering of InP/ZnS core/shell quantum dots by the buffer monolayer for exceptional photocatalytic H<sub>2</sub> evolution. *J. Mater. Chem. A* **2023**, *11*, 6217–6225. [[CrossRef](#)]
42. Jin, N.; Sun, Y.; Shi, W.; Wang, P.; Nagaoka, Y.; Cai, T.; Wu, R.; Dube, L.; Nyiera, H.N.; Liu, Y.; et al. Type-I CdS/ZnS Core/Shell Quantum Dot-Gold Heterostructural Nanocrystals for Enhanced Photocatalytic Hydrogen Generation. *J. Am. Chem. Soc.* **2023**, *145*, 21886–21896. [[CrossRef](#)]
43. Kang, C.; Prodanov, M.F.; Gao, Y.; Mallem, K.; Yuan, Z.; Vashchenko, V.V.; Srivastava, A.K. Quantum-Rod On-Chip LEDs for Display Backlights with Efficacy of 149 lm W<sup>-1</sup>: A Step toward 200 lm W<sup>-1</sup>. *Adv. Mater.* **2021**, *33*, 2104685–2104694. [[CrossRef](#)]
44. Jawhar, N.N.; Soheyli, E.; Yazici, A.F.; Mutlugun, E.; Sahraei, R. Preparation of highly emissive and reproducible Cu–In–S/ZnS core/shell quantum dots with a mid-gap emission character. *J. Alloys Compd.* **2020**, *824*, 153906–153915. [[CrossRef](#)]
45. Weigert, F.; Müller, A.; Häusler, I.; Geißler, D.; Skroblin, D.; Krumrey, M.; Unger, W.; Radnik, J.; Resch-Genger, U. Combining HR-TEM and XPS to elucidate the core–shell structure of ultrabright CdSe/CdS semiconductor quantum dots. *Sci. Rep.* **2020**, *10*, 20712–20725. [[CrossRef](#)]
46. Song, J.; Jiang, T.; Guo, T.; Liu, L.; Wang, H.; Xia, T.; Zhang, W.; Ye, X.; Yang, M.; Zhu, L.; et al. Facile Synthesis of Water-Soluble Zn-Doped AgIn<sub>5</sub>S<sub>8</sub>/ZnS Core/Shell Fluorescent Nanocrystals and Their Biological Application. *Inorg. Chem.* **2015**, *54*, 1627–1633. [[CrossRef](#)]
47. Chen, S.; Ahmadiantehrani, M.; Zhao, J.; Zhu, S.; Mamalis, A.G.; Zhu, X. Heat-up synthesis of Ag–In–S and Ag–In–S/ZnS nanocrystals: Effect of indium precursors on their optical properties. *J. Alloys Compd.* **2016**, *665*, 137–143. [[CrossRef](#)]
48. Dai, J.; Zhang, X. Chemical Regulation of Fluorescence Lifetime. *Chem. Biomed. Imaging* **2023**, *1*, 796–816. [[CrossRef](#)]
49. Wang, Y.; Nie, Z.; Wang, F. Modulation of photocarrier relaxation dynamics in two-dimensional semiconductors. *Light Sci. Appl.* **2020**, *9*, 192–207. [[CrossRef](#)] [[PubMed](#)]
50. May, B.M.; Bambo, M.F.; Hosseini, S.S.; Sidwaba, U.; Nxumalo, E.N.; Mishra, A.K. A review on I–III–VI ternary quantum dots for fluorescence detection of heavy metals ions in water: Optical properties, synthesis and application. *RSC Adv.* **2022**, *12*, 11216–11232. [[CrossRef](#)]
51. Deng, B.; Yang, Y.; Khan, A.U.; Chen, Q.; Wang, X.; Ren, T.; Li, J.; Liu, Y.; Li, L.; Mao, B. In Situ Preparation of 0D/2D Zn–Ag–In–S Quantum Dots/RGO Heterojunctions for Efficient Photocatalytic Hydrogen Production. *Catalysts* **2023**, *13*, 1471. [[CrossRef](#)]
52. Wang, W.; Li, B.; Yang, H.-J.; Liu, Y.; Gurusamy, L.; Karuppasamy, L.; Wu, J.J. Photocatalytic Hydrogen Evolution from Water Splitting Using Core-Shell Structured Cu/ZnS/COF Composites. *Nanomaterials* **2021**, *11*, 3380. [[CrossRef](#)] [[PubMed](#)]
53. Su, J.; Zhang, T.; Wang, L.; Shi, J.; Chen, Y. Surface treatment effect on the photocatalytic hydrogen generation of CdS/ZnS core-shell microstructures. *Chin. J. Catal.* **2017**, *38*, 489–497. [[CrossRef](#)]
54. Liu, X.; Zhang, Y.; Matsushima, S.; Sugiyama, T.; Hojo, H.; Einaga, H. Rational Design of Cu-Doped ZnS Nanospheres for Photocatalytic Evolution of H<sub>2</sub> with Visible Light. *ACS Appl. Energy Mater.* **2022**, *5*, 1849–1857. [[CrossRef](#)]
55. Xu, X.; Zhang, J.; Wang, S.; Yao, Z.; Wu, H.; Shi, L.; Yin, Y.; Wang, S.; Sun, H. Photocatalytic reforming of biomass for hydrogen production over ZnS nanoparticles modified carbon nitride nanosheets. *J. Colloid Interface Sci.* **2019**, *555*, 22–30. [[CrossRef](#)] [[PubMed](#)]
56. Kang, H.; Kim, J.H. Utilization of a ZnS(en)<sub>0.5</sub> photocatalyst hybridized with a CdS component for solar energy conversion to hydrogen. *Adv. Powder Technol.* **2017**, *28*, 2438–2444. [[CrossRef](#)]
57. Zhang, S.; Ou, X.; Xiang, Q.; Carabineiro, S.A.C.; Fan, J.; Lv, K. Research progress in metal sulfides for photocatalysis: From activity to stability. *Chemosphere* **2022**, *303*, 135085. [[CrossRef](#)]
58. Caudillo-Flores, U.; Fuentes-Moyado, S.; Alonso-Núñez, G.; Barba-Nieto, I.; Fernández-García, M.; Kubacka, A. Pd–Sn promoted NbO<sub>x</sub>/TiO<sub>2</sub> catalysts for hydrogen photoproduction: Effect of Pd–Sn interaction on charge handling and reaction mechanism. *Chem. Eng. J.* **2023**, *457*, 141134. [[CrossRef](#)]
59. Caudillo-Flores, U.; Fuentes-Moyado, S.; Fernández-García, M.; Kubacka, A. Effect of niobium on the performance of Pd–TiO<sub>2</sub> photocatalysts for hydrogen production. *Catal. Today* **2023**, *419*, 114147. [[CrossRef](#)]

**Disclaimer/Publisher’s Note:** The statements, opinions and data contained in all publications are solely those of the individual author(s) and contributor(s) and not of MDPI and/or the editor(s). MDPI and/or the editor(s) disclaim responsibility for any injury to people or property resulting from any ideas, methods, instructions or products referred to in the content.